Lattice realizations of unitary minimal modular invariant partition functions

1995 J. Phys. A: Math. Gen. 28 4891

(http://iopscience.iop.org/0305-4470/28/17/020)

J. Phys. A: Math. Gen. 28 (1995) 4891–4905. Printed in the UK

Lattice realizations of unitary minimal modular invariant partition functions

David L O'Brien† and Paul A Pearce‡

Mathematics Department, University of Melbourne, Parkville, Victoria 3052, Australia

Received 17 March 1995

Abstract. The conformal spectra of the critical dilute A–D–E lattice models are studied numerically. The results strongly indicate that, in branches one and two, these models provide realizations of the complete A–D–E classification of unitary minimal modular invariant partition functions given by Cappelli, Itzykson and Zuber. In branches three and four the results indicate that the modular invariant partition functions factorize. Similar factorization results are also obtained for two-colour lattice models.

1. Introduction

It is well established that the critical behaviour of two-dimensional lattice models is described by conformal field theory or, to put it another way, that the continuum limits of critical lattice models provide realizations of two-dimensional conformal field theories. An important class of conformal field theories is the unitary minimal series with central charge $c < 1$. In this case a complete A–D–E classification of the theories has been obtained by Cappelli *et al* [1]. In this paper we present compelling numerical evidence to show that the critical dilute A–D–E lattice models [2–4] provide realizations of this complete A–D–E classification of unitary minimal conformal field theories, as conjectured by Roche [3]. The layout of the paper is as follows. In section 2 we describe the minimal conformal field theories and their A–D–E classification. In section 3 we define the critical A–D–E models due to Pasquier [5] and their dilute and two-colour [6] generalizations. We also summarize the conjectured modular invariant partition functions for these models. Finally, in section 4 we present the numerical results that confirm the conjectured modular invariant partition functions.

2. Conformal field theory

2.1. Minimal models

In 1984 Belavin *et al* [7] introduced the minimal series of conformally invariant field theories. These models are characterized by a central charge $c < 1$ which is restricted to the discrete values

$$c = 1 - \frac{6(p - p')^2}{pp'} \tag{2.1}$$

† E-mail address: dlo@maths.mu.oz.au

‡ E-mail address: pap@maths.mu.oz.au

0305-4470/95/174891+15$19.50

with p and p' coprime positive integers. The conformal weights of the minimal series are given by the Kac formula

$$\Delta = \Delta_{r,s}^{(p,p')} = \frac{(rp' - sp)^2 - (p' - p)^2}{4pp'} \tag{2.2}$$

with

$$1 \leqslant r \leqslant p - 1 \qquad 1 \leqslant s \leqslant p' - 1. \tag{2.3}$$

Moreover, Friedan *et al* [8] showed that if the theory is unitary, then the central charge is further restricted by $|p - p'| = 1$, and if in fact $p' - p = 1$ then

$$c = 1 - \frac{6}{p'(p' - 1)} \qquad p' = 4, 5, 6, \ldots. \tag{2.4}$$

The grids of conformal weights for $p' = 4, 5$ and 6 are shown in figure 1.

$p' = 4$

s		
3	1/2	0
2	1/16	1/16
1	0	1/2
	1	2 r

$p' = 5$

s			
4	3/2	7/16	0
3	3/5	3/80	1/10
2	1/10	3/80	3/5
1	0	7/16	3/2
	1	2	3 r

$p' = 6$

s				
5	3	7/5	2/5	0
4	13/8	21/40	1/40	1/8
3	2/3	1/15	1/15	2/3
2	1/8	1/40	21/40	13/8
1	0	2/5	7/5	3
	1	2	3	4 r

Figure 1. Grids of conformal weights for the unitary minimal models with $p' = 4, 5, 6$ and $p = p' - 1$. The table with $p' = 4$, $c = 1/2$ is identified with the Ising model, $p' = 5$, $c = 7/10$ is identified with the tri-critical Ising model and $p' = 6$, $c = 4/5$ with the tetra-critical Ising model. The odd rows of the $p' = 6$ Kac table give the critical exponents of the three-state Potts model.

2.2. *A–D–E classification of modular invariant partition functions*

For a conformal field theory on a torus, modular invariance [9] implies further constraints on the theory. The requirement of modular invariance is strong enough to fix the operator content. In fact, Cappelli *et al* [1] have obtained a complete classification of minimal modular invariant partition functions. Remarkably, they obtain two series in one-to-one correspondence with the *A–D–E* classical Lie algebras, one labelled by (A, G) and the other by (G, A), with Coxeter numbers (p, p') in each case, and $p' > p$. The *A–D–E* classification of minimal modular invariant partition functions is shown in table 1. The Virasoro characters in this table are defined by

Table 1. *A–D–E* classification of minimal modular invariant partition functions. The central charges are $c = 1 - 6(p-p')^2/pp'$, $\chi_{r,s} = \chi_{r,s}(q)$ are Virasoro characters and bars denote complex conjugates. In this series r, s are Coxeter exponents of (A, G). There is a second series where r, s are Coxeter exponents of (G, A). In both series $p' > p$, and the unitary minimal models have $p' - p = 1$.

(A, G)	Modular invariant partition function
$(A_{p-1}, A_{p'-1})$	$Z = \frac{1}{2}\sum_{r=1}^{p-1}\sum_{s=1}^{p'-1}\lvert\chi_{r,s}\rvert^2$
$(A_{p-1}, D_{2\rho+2})$ $p'=4\rho+2\geqslant 6$	$Z = \frac{1}{2}\sum_{r=1}^{p-1}\left\{\sum_{\substack{s=1\\ s\ \text{odd}}}^{2\rho-1}\lvert\chi_{r,s}+\chi_{r,4\rho+2-s}\rvert^2 + 2\lvert\chi_{r,2\rho+1}\rvert^2\right\}$
$(A_{p-1}, D_{2\rho+1})$ $p'=4\rho\geqslant 8$	$Z = \frac{1}{2}\sum_{r=1}^{p-1}\left\{\sum_{\substack{s=1\\ s\ \text{odd}}}^{4\rho-1}\lvert\chi_{r,s}\rvert^2 + \lvert\chi_{r,2\rho}\rvert^2 + \sum_{\substack{s=2\\ s\ \text{even}}}^{2\rho-2}(\chi_{r,s}\bar{\chi}_{r,4\rho-s}+\bar{\chi}_{r,s}\chi_{r,4\rho-s})\right\}$
(A_{p-1}, E_6) $p'=12$	$Z = \frac{1}{2}\sum_{r=1}^{p-1}\left\{\lvert\chi_{r,1}+\chi_{r,7}\rvert^2 + \lvert\chi_{r,4}+\chi_{r,8}\rvert^2 + \lvert\chi_{r,5}+\chi_{r,11}\rvert^2\right\}$
(A_{p-1}, E_7) $p'=18$	$Z = \frac{1}{2}\sum_{r=1}^{p-1}\left\{\lvert\chi_{r,1}+\chi_{r,17}\rvert^2 + \lvert\chi_{r,5}+\chi_{r,13}\rvert^2 + \lvert\chi_{r,7}+\chi_{r,11}\rvert^2 + \lvert\chi_{r,9}\rvert^2 + [(\chi_{r,3}+\chi_{r,15})\bar{\chi}_{r,9} + (\bar{\chi}_{r,3}+\bar{\chi}_{r,15})\chi_{r,9}]\right\}$
(A_{p-1}, E_8) $p'=30$	$Z = \frac{1}{2}\sum_{r=1}^{p-1}\left\{\lvert\chi_{r,1}+\chi_{r,11}+\chi_{r,19}+\chi_{r,29}\rvert^2 + \lvert\chi_{r,7}+\chi_{r,13}+\chi_{r,17}+\chi_{r,23}\rvert^2\right\}$

$$\chi_{r,s}(q) = \frac{q^{-c/24+\Delta_{r,s}^{(p,p')}}}{Q(q)}\sum_{n=-\infty}^{\infty}\left\{q^{n(npp'+rp'-sp)} - q^{(np'+s)(np+r)}\right\} \tag{2.5}$$

where q is the modular parameter and

$$Q(q) = \prod_{n=1}^{\infty}(1-q^n). \tag{2.6}$$

Here we are primarily interested in the unitary minimal models with $p' - p = 1$. In this case the two *A–D–E* series correspond to

$$(A, G) = \begin{cases}(A_{p'-2}, A_{p'-1})\\ (A_{p'-2}, D_{(p'+2)/2})\\ (A_{10}, E_6)\\ (A_{16}, E_7)\\ (A_{28}, E_8)\end{cases} \qquad (G, A) = \begin{cases}(A_{p-1}, A_p)\\ (D_{(p+2)/2}, A_p)\\ (E_6, A_{12})\\ (E_7, A_{18})\\ (E_8, A_{30})\end{cases} \tag{2.7}$$

with central charges

$$c = 1 - \frac{6}{p'(p'-1)} = 1 - \frac{6}{p(p+1)}. \tag{2.8}$$

The Coxeter numbers and the Coxeter exponents of the classical *A–D–E* Lie algebras are shown in table 2. The Dynkin diagrams are shown in figure 2. Some members of these series are identified as

$$\begin{aligned}&(A_2, A_3) = \text{critical Ising} && c = 1/2\\ &(A_4, D_4) = \text{critical three-state Potts} && c = 4/5\\ &(A_3, A_4) = \text{tri-critical Ising} && c = 7/10\\ &(D_4, A_6) = \text{tri-critical three-state Potts} && c = 6/7.\end{aligned} \tag{2.9}$$

For this reason we will refer to the (A, G) series as the critical series and the (G, A) series as the tri-critical series. In particular, the modular invariant partition functions of the critical and tri-critical three-state Potts models are

$$(A_4, D_4) : Z = \frac{1}{2}\sum_{r=1}^{4}\left\{|\chi_{r,1} + \chi_{r,5}|^2 + 2|\chi_{r,3}|^2\right\} \qquad (p = 5, p' = 6) \tag{2.10}$$

$$(D_4, A_6) : Z = \frac{1}{2}\sum_{s=1}^{6}\left\{|\chi_{1,s} + \chi_{5,s}|^2 + 2|\chi_{3,s}|^2\right\} \qquad (p = 6, p' = 7). \tag{2.11}$$

Table 2. The Coxeter number h and Coxeter exponents s of the classical A–D–E Lie algebras.

G	h	s
A_L	$L+1$	$1, 2, 3, \ldots, L$
D_L	$2L-2$	$L-1, 1, 3, 5, \ldots, 2L-3$
E_6	12	1, 4, 5, 7, 8, 11
E_7	18	1, 5, 7, 9, 11, 13, 17
E_8	30	1, 7, 11, 13, 17, 19, 23, 29

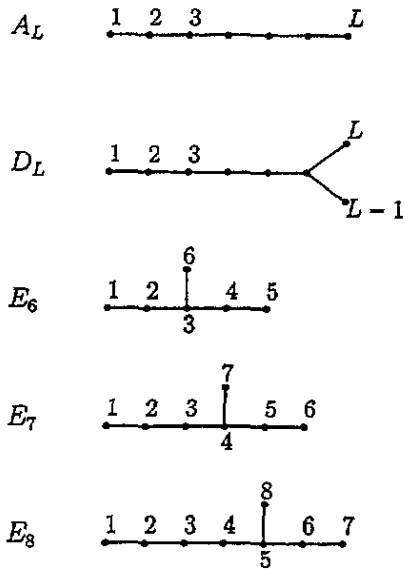

Figure 2. The Dynkin diagrams of the classical A–D–E Lie algebras. The A–D–E graphs classify all connected graphs whose associated adjacency matrices have eigenvalues strictly less than two. The eigenvalues of the adjacency matrices are, in fact, given by $2\cos(s\pi/h)$ where s ranges over the Coxeter exponents.

The A–D–E classification of unitary minimal conformal field theories gives an exhaustive list of theories with $c < 1$. In other words, this is a complete list of universality classes giving all possible critical behaviours for two-dimensional statistical systems with $c < 1$. A natural question to ask is whether a solvable lattice model can be found as a representative of each universality class allowed by the A–D–E classification.

3. *A–D–E* lattice models and their modular invariant partition functions

3.1. Pasquier's A–D–E models

By a remarkable coincidence, in the same year that Belavin *et al* introduced the minimal conformal field theories, Andrews, Baxter and Forrester (ABF) [10] solved the first infinite hierarchy of lattice models in the form of restricted solid-on-solid (RSOS) models. The spins in these models take values on the A_L Dynkin diagram and are subject to the constraint that the state of adjacent spins on the square lattice must be adjacent on the A_L diagram. Huse [11] showed that the critical behaviour of these L height RSOS models is precisely described by the unitary minimal series. Moreover, it turns out that the modular invariant partition functions of the ABF RSOS models give the (A_{L-1}, A_L) series with $L = 3, 4, 5, \ldots$.

The lattice realizations of this critical series of modular invariant partition functions were completed in 1987 by Pasquier [5] who generalized the ABF models by constructing solvable lattice models whose states take values on the A–D–E graphs. The A_L models of Pasquier are just the critical ABF RSOS models. We note that, although the A and D models admit off-critical elliptic extensions, the exceptional E models can only be solved at criticality. The face weights of Pasquier's critical A–D–E models are given by

$$W\left(\begin{matrix} d & c \\ a & b \end{matrix}\middle| u\right) = \begin{array}{ccc} & d & \\ a & u & c \\ & b & \end{array} = \frac{\sin(\lambda - u)}{\sin\lambda}\delta_{a,c}A_{a,b}A_{a,d} + \frac{\sin u}{\sin\lambda}\sqrt{\frac{S_aS_c}{S_bS_d}}\delta_{b,d}A_{a,b}A_{b,c} \tag{3.1}$$

where the spins a, b, c, d take values on the given A–D–E graph. The parameter u is called the spectral parameter. In the branches of interest here, the spectral parameter lies in the interval $0 < u < \lambda$. The adjacency matrices are given by

$$A_{a,b} = \begin{cases} 1 & a, b \text{ connected} \\ 0 & \text{otherwise.} \end{cases} \tag{3.2}$$

The non-negative components S_a of the Perron–Frobenius eigenvector are determined by

$$\sum_b A_{a,b}S_b = 2\cos\lambda S_a \tag{3.3}$$

where $2\cos\lambda$ is the largest eigenvalue of the adjacency matrix and

$$\lambda = \pi/h \tag{3.4}$$

is called the crossing parameter. The Coxeter number h is given in table 2.

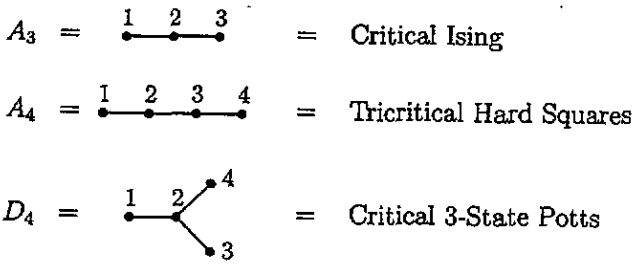

Figure 3. Some prototype classical A–D–E lattice models.

Pasquier's A–D–E models include some much studied models in statistical mechanics; some prototypes are shown in figure 3. The modular invariant partition functions of Pasquier's critical A–D–E models precisely realize the (A, G) series of Cappelli *et al*. However, for many years realizations of the (G, A) series were missing.

3.2. Dilute A–D–E models

In 1992 Warnaar *et al* [2] and Roche [3] independently obtained a second series of solvable lattice models whose states take values on the A–D–E graphs. These lattice models are called the dilute A–D–E models. The face weights of the dilute A–D–E lattice models at criticality are given by

$$W\left(\begin{matrix} d & c \\ a & b \end{matrix}\middle| u\right) = \rho_1(u)\delta_{a,b,c,d} + \rho_2(u)\delta_{a,b,c}A_{a,d} + \rho_3(u)\delta_{a,c,d}A_{a,b} + \sqrt{\frac{S_a}{S_b}}\rho_4(u)\delta_{b,c,d}A_{a,b}$$
$$+\sqrt{\frac{S_c}{S_a}}\rho_5(u)\delta_{a,b,d}A_{a,c} + \rho_6(u)\delta_{a,b}\delta_{c,d}A_{a,c} + \rho_7(u)\delta_{a,d}\delta_{c,b}A_{a,b}$$
$$+\rho_8(u)\delta_{a,c}A_{a,b}A_{a,d} + \sqrt{\frac{S_aS_c}{S_bS_d}}\rho_9(u)\delta_{b,d}A_{a,b}A_{b,c} \tag{3.5}$$

where, as before, the adjacency matrix is

$$A_{a,b} = \begin{cases} 1 & a, b \text{ adjacent} \\ 0 & \text{otherwise} \end{cases} \tag{3.6}$$

and the Perron–Frobenius vector is given by

$$\sum_b A_{a,b}S_b = 2\cos\left(\frac{\pi}{h}\right)S_a. \tag{3.7}$$

The effective adjacency graph is given by adding a loop to each node of the A–D–E graphs, that is, the spin states at adjacent sites of the lattice are either the same or adjacent on the A–D–E graph. The generalized Kronecker delta is

$$\delta_{a,b,c,\ldots} = \begin{cases} 1 & a = b = c = \ldots \\ 0 & \text{otherwise} \end{cases} \tag{3.8}$$

and the trigonometric weight functions are

$$\rho_1(u) = 1 + \frac{\sin u \sin(3\lambda - u)}{\sin(2\lambda)\sin(3\lambda)} \qquad \rho_2(u) = \rho_3(u) = \frac{\sin(3\lambda - u)}{\sin(3\lambda)}$$
$$\rho_4(u) = \rho_5(u) = \epsilon\frac{\sin u}{\sin(3\lambda)} \qquad \rho_6(u) = \rho_7(u) = \epsilon\frac{\sin u \sin(3\lambda - u)}{\sin(2\lambda)\sin(3\lambda)} \tag{3.9}$$
$$\rho_8(u) = \frac{\sin(2\lambda - u)\sin(3\lambda - u)}{\sin(2\lambda)\sin(3\lambda)} \qquad \rho_9(u) = -\frac{\sin u \sin(\lambda - u)}{\sin(2\lambda)\sin(3\lambda)}.$$

Here $\epsilon = \pm 1$; the choices $\epsilon = 1$ in the $u > 0$ branches and $\epsilon = -1$ in the $u < 0$ branches ensure positive Boltzmann weights at the isotropic points $u = \gamma/2$.

The dilute A–D–E models are solvable for two choices of λ:

$$\lambda = \begin{cases} \dfrac{(h-1)\pi}{4h} & \text{branches one and four} \\ \dfrac{(h+1)\pi}{4h} & \text{branches two and three.} \end{cases} \tag{3.10}$$

The physical branches are summarized in table 3. The central charges of these models in branches one and two are given by [2, 4, 12, 13]

$$c = \begin{cases} 1 - \dfrac{6}{h(h+1)} & \text{branch one} \\ 1 - \dfrac{6}{h(h-1)} & \text{branch two.} \end{cases} \tag{3.11}$$

Table 3. Physical branches and central charges of the dilute A–D–E lattice models.

	Crossing parameter	Inversion point	Physical region	Central charge
Branch one	$\lambda = \frac{\pi}{4}\left(1 - \frac{1}{h}\right)$	$\gamma = 3\lambda$	$u \in (0, \gamma)$	$c = 1 - \frac{6}{h(h+1)}$
Branch two	$\lambda = \frac{\pi}{4}\left(1 + \frac{1}{h}\right)$	$\gamma = 3\lambda$	$u \in (0, \gamma)$	$c = 1 - \frac{6}{h(h-1)}$
Branch three	$\lambda = \frac{\pi}{4}\left(1 + \frac{1}{h}\right)$	$\gamma = 3\lambda - \pi$	$u \in (\gamma, 0)$	$c = \frac{3}{2} - \frac{6}{h(h+1)}$
Branch four	$\lambda = \frac{\pi}{4}\left(1 - \frac{1}{h}\right)$	$\gamma = 3\lambda - \pi$	$u \in (\gamma, 0)$	$c = \frac{3}{2} - \frac{6}{h(h-1)}$

This suggests identifying the universality classes of the first few dilute A–D–E models as

$$\begin{aligned} &\text{branch two}: A_3 = \text{critical Ising} \qquad c = 1/2 \\ &\text{branch one}: A_3 = \text{tri-critical Ising} \qquad c = 7/10 \\ &\text{branch two}: D_4 = \text{critical three-state Potts} \qquad c = 4/5 \\ &\text{branch one}: D_4 = \text{tri-critical three-state Potts} \qquad c = 6/7. \end{aligned} \tag{3.12}$$

Notice that the dilute A_3 and D_4 are not the usual Ising and three-state Potts models, they just have the same $\mathbb{Z}_2$ and $\mathbb{Z}_3$ symmetries and lie in the same universality classes.

The dilute A–D–E lattice models in branch two do, in fact, give a second realization of the (A, G) series of Cappelli *et al.* More importantly, as we show in the next section, the dilute A–D–E lattice models in branch one precisely realize the missing (G, A) series. The dilute A–D–E models thus give a complete realization of all unitary minimal conformal field theories.

3.3. Two-colour A–D–E models

The two-colour models, obtained by Warnaar and Nienhuis [6], are dense RSOS models built on pairs of A–D–E adjacency graphs. Each site on the lattice carries two heights, one from each graph. In moving between adjacent sites, one of the heights remains constant and the other varies as permitted by its corresponding adjacency graph. If G^1 and G^2 are the adjacency matrices of the two graphs, the effective adjacency matrix of the two-colour model is, therefore, $A = A^1 + A^2$, where

$$A^1 = G^1 \otimes I \qquad A^2 = I \otimes G^2 \tag{3.13}$$

With a slight abuse of notation we will denote such a model by $G^1 \otimes G^2$. The Perron–Frobenius vector of A is the tensor product $S = S^1 \otimes S^2$ of the Perron–Frobenius vectors of the underlying graphs. In constructing the two-colour models it is assumed that the graphs G^1 and G^2 have the same largest eigenvalue and hence the same Coxeter numbers.

Explicitly, the state at each site is given by an ordered pair $a = (a_1, a_2)$ so that

$$S_a = S^1_{a_1} S^2_{a_2} \tag{3.14}$$

$$A^i_{a,b} = G^i_{a_i,b_i} \delta_{a_{3-i},b_{3-i}}. \tag{3.15}$$

In terms of these entities, the face weights of the critical lattice model are given by

$$W\left(\begin{matrix} d & c \\ a & b \end{matrix}\middle| u\right) = \sum_{i=1}^{2} \left[\rho_1(u) A^i_{a,b} A^{3-i}_{b,c} A^i_{c,d} A^{3-i}_{d,a} + \delta_{a,c} \left(\rho_2(u) A^i_{a,b} A^i_{a,d} + \rho_3(u) A^i_{a,b} A^{3-i}_{a,d} \right) \right.$$
$$\left. + \sqrt{\frac{S_a S_c}{S_b S_d}}\, \delta_{b,d} \left(\rho_4(u) A^i_{a,b} A^{3-i}_{b,c} + \rho_5(u) A^{3-i}_{a,b} A^i_{b,c} \right) \right] \tag{3.16}$$

where

$$\begin{aligned}
\rho_1(u) &= \epsilon \frac{\sin u \sin(3\lambda - u)}{\sin\lambda \sin 3\lambda} \\
\rho_2(u) &= \frac{\sin(\lambda - u)\sin(3\lambda - u)}{\sin\lambda \sin 3\lambda} \\
\rho_3(u) &= \frac{\sin(3\lambda - u)}{\sin 3\lambda} \\
\rho_4(u) &= -\frac{\sin u \sin(2\lambda - u)}{\sin\lambda \sin 3\lambda} \\
\rho_5(u) &= -\epsilon \frac{\sin u}{\sin 3\lambda}.
\end{aligned} \tag{3.17}$$

Table 4. Physical branches and central charges of the two-colour A–D–E lattice models.

	Crossing parameter	Inversion point	Physical region	Central charge
Branch one	$\lambda = \frac{\pi}{2}\left(1 - \frac{1}{h}\right)$	$\gamma = 3\lambda - \pi$	$u \in (0, \gamma)$	$c = 2\left(1 - \frac{6}{h(h+1)}\right)$
Branch two	$\lambda = \frac{\pi}{2}\left(1 - \frac{1}{h}\right)$	$\gamma = 3\lambda - 2\pi$	$u \in (\gamma, 0)$	$c = 2\left(1 - \frac{6}{h(h-1)}\right)$

The two-colour models have two physical regimes as summarized in table 4 in terms of the Coxeter number h of the underlying graphs. The choice of the sign factor $\epsilon = \pm 1$ such that $\epsilon = 1$ in branch I and $\epsilon = -1$ in branch two ensures that the Boltzmann weights are positive at the isotropic points $u = \gamma/2$.

3.4. Conjectured modular invariant partition functions

The partition function of a critical lattice model on a finite $\ell \times \ell'$ periodic lattice or torus can be written as

$$Z_{\ell,\ell'} \sim \exp(-\ell\ell' f) Z(q) \tag{3.18}$$

where f is the bulk free energy and $Z(q)$ is a universal term describing the leading finite-size corrections in the limit of ℓ, ℓ' large with the aspect ratio $\delta = \ell'/\ell$ fixed. The argument q is the modular parameter. For a spatially isotropic model, it is simply related to the aspect ratio δ by $q = \exp(-2\pi\delta)$.

The modular invariant partition functions of the dilute A–D–E models built on the classical graph G with Coxeter number h are conjectured to be

$$\begin{aligned}
&\text{branch one} : (G, A_h) && \text{branch two} : (A_{h-2}, G) \\
&\text{branch three} : (G, A_h) \times (A_2, A_3) && \text{branch four} : (A_{h-2}, G) \times (A_2, A_3).
\end{aligned} \tag{3.19}$$

Here the modular parameter is

$$q = \exp(2\pi i\tau) \qquad \tau = \frac{\ell'}{\ell} \exp[i(\pi - \theta)] \tag{3.20}$$

and the effective angle θ [14] is given by

$$\theta = \begin{cases} \dfrac{\pi u}{3\lambda} & \text{branches one and two} \\ \dfrac{\pi u}{3\lambda - \pi} & \text{branches three and four.} \end{cases} \tag{3.21}$$

The modular invariant partition functions of the two-colour A–D–E models are conjectured to be as follows, where once again h is the Coxeter number of the underlying graphs G^1 and G^2:

branch one : $(G^1, A_h) \times (G^2, A_h)$ branch two : $(A_{h-2}, G^1) \times (A_{h-2}, G^2)$.

Here the modular parameter q is as before, but now the effective angle is

$$\theta = \begin{cases} \dfrac{\pi u}{3\lambda - \pi} & \text{branch one} \\ \dfrac{\pi u}{3\lambda - 2\pi} & \text{branch two.} \end{cases} \tag{3.22}$$

4. Numerical results

The central charges and scaling dimensions of critical lattice models can be extracted [15] from the finite-size corrections to the eigenvalues of the row transfer matrices

$$\langle a|T(u)|b\rangle = \prod_{j=1}^{N} W\left(\begin{matrix} b_j & b_{j+1} \\ a_j & a_{j+1} \end{matrix}\middle| u\right). \tag{4.1}$$

Specifically, the finite-size corrections to the largest eigenvalue Λ_0 of a periodic transfer matrix with N faces take the form

$$\frac{1}{N}\log\Lambda_0(u) = -f(u) + \frac{\pi c}{6N^2}\sin\theta(u) + o\left(\frac{1}{N^2}\right) \tag{4.2}$$

where f is the free energy, c is the central charge and $\theta(u)$ is the effective angle as defined in section 3.4. At an isotropic point for a square ordered phase, u is fixed such that $\theta = \pi/2$. The finite-size corrections to the next-largest eigenvalues Λ_n with $n = 1, 2, 3, \ldots$ take the form

$$\frac{1}{N}\log\Lambda_n(u) = -f(u) + \frac{2\pi}{N^2}\left[\left(\frac{c}{12} - x_n\right)\sin\theta(u) - is_n\cos\theta(u)\right] + o\left(\frac{1}{N^2}\right) \tag{4.3}$$

where $x_n = \Delta + \overline{\Delta}$ and $s_n = \Delta - \overline{\Delta}$ are respectively the scaling dimension and spin. The scaling dimension takes fractional values, whereas the spin is restricted to integer values.

The free energies of the dilute and two-colour models are calculated by solving the appropriate inversion relations

$$\kappa(u)\kappa(-u) = \rho(u)\rho(-u) \qquad \kappa(u) = \kappa(\gamma - u) \tag{4.4}$$

where $f(u) = -\log\kappa(u)$ is the free energy and

$$\rho(u) = \begin{cases} \dfrac{\sin(2\lambda - u)\sin(3\lambda - u)}{\sin 2\lambda \sin 3\lambda} & \text{dilute models} \\ \dfrac{\sin(\lambda - u)\sin(3\lambda - u)}{\sin\lambda \sin 3\lambda} & \text{two-colour models.} \end{cases} \tag{4.5}$$

The free energy of the critical dilute models is given by [4]

$$f(u) = -2\int_{-\infty}^{\infty} \frac{\cosh(\pi - 5\lambda)x \cosh\lambda x \sinh(\gamma - u)x \sinh ux}{x \sinh\pi x \cosh\gamma x}\,dx \tag{4.6}$$

and the free energy of the critical two-colour models is given by

$$f(u) = -2\int_{-\infty}^{\infty} \frac{\cosh(\pi - 2\lambda)x \cosh 2(\pi - 2\lambda)x \sinh(\gamma - u)x \sinh ux}{x \sinh\pi x \cosh\gamma x}\,dx. \tag{4.7}$$

In these expressions γ is the inversion point in the appropriate branch. The dilute and two-colour models have, respectively, four and two critical branches. Tables 3 and 4 summarize

the crossing parameters, inversion points and central charges in each of the physical branches in terms of the Coxeter numbers h of the underlying graphs as given in table 2.

Given the free energy, the central charge c is estimated by calculating a sequence of largest eigenvalues Λ_0 for increasing values of N and applying a suitable extrapolation scheme. Once the central charge is determined, (4.3) then allows estimation of the scaling dimensions by a similar procedure using the next-largest eigenvalues Λ_n. To obtain accurate values for the central charges and scaling dimensions we need to calculate eigenvalues for N as large as possible. It is, therefore, convenient to prediagonalize the transfer matrices into block diagonal form using the eigenvectors of the shift operator $\Omega = \boldsymbol{T}(0)$ and, in the case of the A and D models, the reflection operator $\boldsymbol{R}$ which arises from the $\mathbb{Z}_2$ symmetry of the A and D Dynkin diagrams. Taken together, these operators reduce the transfer matrices to $2N$ diagonal blocks.

Once a sequence of eigenvalues for increasing N is obtained, equations (4.2) and (4.3) imply that, for large N, the graph of $(\log \Lambda_n/N + f)$ against $1/N^2$ should approximate a line through the origin. However, since the $o(N^{-2})$ corrections tend to vanish fairly slowly, a parabolic fit gives better results. A simple extrapolation scheme to extract the $1/N$ term is to discard all but the last two eigenvalues in the sequence and take the linear coefficient of the parabola passing through these two points and the origin. We have performed this calculation to find numerically the central charges of a variety of dilute and two-colour models as well as the scaling dimensions of the dilute A_3, A_4, D_4, and two-colour $A_4 \otimes A_4$ models. The approximate central charges are summarized in tables 5–7 and the approximate scaling dimensions are summarized in tables 8–14.

Table 5. Central charges of the dilute A–D–E lattice models in the $u > 0$ branches. The numerical approximations are in excellent agreement with the exact values [2] summarized in table 3.

	Branch one			Branch two			
Model	Approx.	Exact		Approx.	Exact		N_{max}
A_3	0.699 999	7/10	0.7	0.500 000	1/2	0.5	12
A_4	0.799 997	4/5	0.8	0.699 997	7/10	0.7	10
A_5, D_4	0.857 140	6/7	0.857 143...	0.799 997	4/5	0.8	10
A_7, D_5	0.916 660	11/12	0.916 666...	0.892 849	25/28	0.892 857...	9
A_{11}, D_7, E_6	0.961 531	25/26	0.961 538...	0.954 536	21/22	0.954 545...	9
A_{17}, D_{10}, E_7	0.982 448	56/57	0.982 456...	0.980 383	50/51	0.980 392...	9

Table 6. Central charges of the dilute A–D–E lattice models in the $u < 0$ branches.

	Branch three			Branch four			
Model	Approx.	Exact		Approx.	Exact		N_{max}
A_3	1.232	6/5	1.2	1.000	1	1	12
A_4	1.327	13/10	1.3	1.199	6/5	1.2	10
A_5, D_4	1.377	19/14	1.357...	1.299	13/10	1.3	10
A_7, D_5	1.432	17/12	1.417...	1.391	39/28	1.393...	8
A_{11}, D_7, E_6	1.470	19/13	1.462...	1.453	16/11	1.455...	8
A_{17}, D_{10}, E_7	1.487	169/114	1.482...	1.479	151/102	1.480...	8

Table 7. Central charges of the two-colour A–D–E lattice models. Here the notation $[G, G']$ means either G or G'. The approximations match well the predictions summarized in table 4.

	Branch one			Branch two			
Model	Approx.	Exact		Approx.	Exact		N_{max}
$A_3 \otimes A_3$	1.423	7/5	1.4	0.9991	1	1	8
$A_4 \otimes A_4$	1.606	8/5	1.6	1.3982	7/5	1.4	8
$[A_5, D_4] \otimes [A_5, D_4]$	1.712	12/7	1.714...	1.5930	8/5	1.6	6
$[A_{11}, D_7, E_6] \otimes [A_{11}, D_7, E_6]$	1.914	25/13	1.923...	1.8993	21/11	1.909...	6

Table 8. Scaling dimensions and multiplicities for the dilute A_3 model in the $u > 0$ branches. We expect branch one to correspond to the partition function labelled by (A_3, A_4) and branch two to that labelled by (A_2, A_3). These correspondences may be verified by comparison of the above approximations to the exact exponents which arise in the partition function expansions of (4.9).

Branch one				Branch two			
Approx.	Exact		Mult.	Approx.	Exact		Mult.
0.074 999 9	3/40	0.075	1	0.125 999	1/8	0.125	1
0.200 000	1/5	0.2	1	0.998 457	1	1	1
0.874 980	7/8	0.875	1	1.124 89	9/8	1.125	2
1.075 05	43/40	1.075	2	2.010 84	2	2	2
1.200 03	6/5	1.2	2	1.988 28	2	2	2
1.199 94	6/5	1.2	1	2.130 60	17/8	2.125	2
1.875 41	15/8	1.875	2				

Table 9. Scaling dimensions and multiplicities for the dilute A_3 model in the $u < 0$ branches. Comparison with the expansions (4.10) shows branch four to be in excellent agreement with the partition function product $(A_2, A_3) \times (A_2, A_3)$, and branch three to be in reasonable agreement with $(A_3, A_4) \times (A_2, A_3)$.

Branch three				Branch four			
Approx.	Exact		Mult.	Approx.	Exact		Mult.
0.0778	3/40	0.075	1	0.1250	1/8	0.125	1
0.1270	1/8	0.125	1	0.1250	1/8	0.125	1
0.2033	1/5	0.2	1	0.2500	1/4	0.25	1
0.2401	1/5	0.2	1	1.0000	1	1	1
				1.0000	1	1	1
				1.1250	9/8	1.125	1
				1.1246	9/8	1.125	2
				1.1248	9/8	1.125	1
				1.1210	9/8	1.125	2
				1.2450	5/4	1.25	2
				1.2424	5/4	1.25	2
				1.9987	2	2	2
				1.9964	2	2	2
				1.9949	2	2	1

The estimates of the scaling dimensions x_n allow the first few terms of the isotropic modular invariant partition functions to be determined, since these partition functions are

Table 10. Scaling dimensions and multiplicities for the dilute A_4 model in the $u > 0$ branches. Branch one agrees well with the expansion (4.9) of the partition function (A_4, A_5), as does branch two with the expansion of (A_3, A_4).

Branch one				Branch two			
Approx.	Exact		Mult.	Approx.	Exact		Mult.
0.050 000	1/20	0.05	1	0.074 999	3/40	0.075	1
0.013 333	2/15	0.133...	1	0.199 997	1/5	0.2	1
0.250 000	1/4	0.25	1	0.873 958	7/8	0.875	1
0.799 969	4/5	0.8	1	1.075 250	43/40	1.075	2
1.050 060	21/20	1.05	2	1.199 460	6/5	1.2	2
1.049 920	21/20	1.05	1	1.196 920	6/5	1.2	1
1.133 360	17/15	1.133...	2				

Table 11. Scaling dimensions and multiplicities for the dilute A_4 model in the $u < 0$ branches. The data for branch four agree very well with the expansion (4.10) of $(A_3, A_4) \times (A_2, A_3)$, and the data for branch 3 agree reasonably with the expansion of $(A_4, A_5) \times (A_2, A_3)$.

Branch three				Branch four			
Approx.	Exact		Mult.	Approx.	Exact		Mult.
0.0501	1/20	0.05	1	0.075 00	3/40	0.075	1
0.1256	1/8	0.125	1	0.125 00	1/8	0.125	1
0.1357	2/15	0.133...	1	0.199 85	1/5	0.2	1
0.1918	7/40	0.175	1	0.200 00	1/5	0.2	1
0.2498	1/4	0.25	1	0.325 00	13/40	0.325	1
				0.875 06	7/8	0.875	1
				0.999 84	1	1	1
				0.998 03	1	1	1
				1.075 08	43/40	1.075	1
				1.098 86	43/40	1.075	2

Table 12. Scaling dimensions and multiplicities for the dilute D_4 model in the $u > 0$ branches. Comparison with the partition function expansions (4.9) shows branch one to correspond to (D_4, A_6), and branch two to (A_4, D_4); these are respectively tri-critical and critical three-state Potts.

Branch one				Branch two			
Approx.	Exact		Mult.	Approx.	Exact		Mult.
0.095 234	2/21	0.095 238...	2	0.133 33	2/15	0.133...	2
0.285 711	2/7	0.285 714...	1	0.798 273	4/5	0.8	1
0.951 915	20/21	0.952 381...	2	1.1335	17/15	1.133...	4
1.095 86	23/21	1.095 24...	4	1.322 42	4/3	1.33...	2
1.285 83	9/7	1.285 71...	2	1.792 66	9/5	1.8	2

simply

$$Z(q) = q^{-c/12}\left(1 + \sum_{n=1}^{\infty} d_n q^{x_n}\right) \tag{4.8}$$

where d_n are the multiplicities. For the dilute models, we see that branches one and two are described by the series of partition functions in table 1 and that the partition functions

Table 13. Scaling dimensions and multiplicities for the dilute D_4 model in the $u < 0$ branches. Branch four agrees well with the expansion (4.10) of $(A_4, D_4) \times (A_2, A_3)$, and branch three agrees reasonably with that of $(D_4, A_6) \times (A_2, A_3)$.

Branch three				Branch four			
Approx.	Exact		Mult.	Approx.	Exact		Mult.
0.096 03	2/21	0.095 24...	2	0.124 50	1/8	0.125	1
0.125 20	1/8	0.125	1	0.133 27	2/15	0.133 33...	2
0.244 14	37/168	0.220 24...	1	0.258 41	31/120	0.258 33...	2
0.244 14	37/168	0.220 24...	1	0.800 06	4/5	0.8	1
0.283 76	2/7	0.285 71...	1	0.925 28	37/40	0.925	1
				0.999 71	1	1	1
				1.116 98	9/8	1.125	2
				1.135 14	17/15	1.133 33...	2

Table 14. Scaling dimensions and multiplicities for the two-colour $A_4 \otimes A_4$ model. These agree well with the partition function expansions of $(A_4, A_5) \times (A_4, A_5)$ in branch one and $(A_3, A_4) \times (A_3, A_4)$ in branch two.

Branch one				Branch two			
Approx.	Exact		Mult.	Approx.	Exact		Mult.
0.0499	1/20	0.05	2	0.0750	3/40	0.075	2
0.1016	1/10	0.1	1	0.1500	3/20	0.15	1
0.1333	2/15	0.133...	2	0.1996	1/5	0.2	2
0.1877	11/60	0.1833...	2	0.2750	11/40	0.275	2
0.2489	1/4	0.25	2	0.4000	2/5	0.4	1
0.2798	4/15	0.266...	1	0.8839	7/8	0.875	2
0.3107	3/10	0.3	2	0.9412	19/20	0.95	2
				1.0807	43/40	1.075	4

in branches three and four are the product of the critical Ising partition function (A_2, A_3) with those of branches one and two respectively.

Dilute A_3, therefore, has the following modular invariant partition functions in its four branches:

branch one : (A_3, A_4) branch two : (A_2, A_3)

branch three : $(A_3, A_4) \times (A_2, A_3)$ branch four : $(A_2, A_3) \times (A_2, A_3)$.

Similarly, dilute A_4 has the partition functions

branch one : (A_4, A_5) branch two : (A_3, A_4)

branch three : $(A_4, A_5) \times (A_2, A_3)$ branch four : $(A_3, A_4) \times (A_2, A_3)$

and dilute D_4 has the partition functions

branch one : (D_4, A_6) branch two : (A_4, D_4)

branch three : $(D_4, A_6) \times (A_2, A_3)$ branch four : $(A_4, D_4) \times (A_2, A_3)$.

The isotropic expansions of these modular invariant partition functions are, to the relevant order,

$$
\begin{aligned}
&(A_2, A_3) : Z(q) = q^{-1/24}\left[1 + q^{1/8} + q + 2q^{9/8} + 4q^2 + O(q^{17/8})\right] \\
&(A_3, A_4) : Z(q) = q^{-7/120}\left[1 + q^{3/40} + q^{1/5} + q^{7/8} + 2q^{43/40} + 3q^{6/5} + O(q^{15/8})\right] \\
&(A_4, A_5) : Z(q) = q^{-1/15}\left[1 + q^{1/20} + q^{2/15} + q^{1/4} + q^{4/5} + 3q^{21/20} + O(q^{17/15})\right] \\
&(A_4, D_4) : Z(q) = q^{-1/15}\left[1 + 2q^{2/15} + q^{4/5} + 4q^{17/15} + 2q^{4/3} + 4q^{9/5} + O(q^2)\right] \\
&(D_4, A_6) : Z(q) = q^{-1/14}\left[1 + 2q^{2/21} + q^{2/7} + 2q^{20/21} + 4q^{23/21} + 2q^{9/7} + O(q^{10/7})\right].
\end{aligned}
\tag{4.9}
$$

The products of each of these with the Ising partition function $Z_I = (A_2, A_3)$ yield

$$
\begin{aligned}
&Z_I \times (A_2, A_3) : Z(q) = q^{-1/12}\left[1 + 2q^{1/8} + q^{1/4} + 2q + 6q^{9/8} + 4q^{5/4} + O(q^2)\right] \\
&Z_I \times (A_3, A_4) : Z(q) = q^{-1/10}\left[1 + q^{3/40} + q^{1/8} + 2q^{1/5}\right. \\
&\qquad \left. + q^{13/40} + q^{7/8} + q + O(q^{43/40})\right] \\
&Z_I \times (A_4, A_5) : Z(q) = q^{-13/120}\left[1 + q^{1/20} + q^{1/8} + q^{2/15}\right. \\
&\qquad \left. + q^{7/40} + q^{1/4} + q^{31/120} + O(q^{3/8})\right] \\
&Z_I \times (A_4, D_4) : Z(q) = q^{-13/120}\left[1 + q^{1/8} + 2q^{2/15} + 2q^{31/120}\right. \\
&\qquad \left. + q^{4/5} + q^{37/40} + q + 2q^{9/8} + O(q^{17/15})\right] \\
&Z_I \times (D_4, A_6) : Z(q) = q^{-19/168}\left[1 + 2q^{2/21} + q^{1/8} + 2q^{37/168} + q^{2/7} + O(q^{23/56})\right].
\end{aligned}
\tag{4.10}
$$

We find that the results for the two-colour models are similar to those of the dilute models. The modular invariant partition functions are all found to be a product of two partition functions in table 1 with the same central charge. Thus, for example, the partition functions of the two-colour model built on the graph $A_4 \otimes A_4$ are given by

$$\text{branch one} : (A_4, A_5) \times (A_4, A_5) \qquad \text{branch two} : (A_3, A_4) \times (A_3, A_4).$$

Our numerical estimates for the scaling dimensions of this model are summarized in table 14. The expansions of the isotropic partition function products are

$$
\begin{aligned}
&\text{branch one} : Z(q) = q^{-2/15}\left[1 + 2q^{1/20} + q^{1/10} + 2q^{2/15} + 2q^{11/60} + 2q^{1/4} + q^{4/15}\right. \\
&\qquad \left. + 2q^{3/10} + O(q^{23/60})\right] \\
&\text{branch two} : Z(q) = q^{-7/60}\left[1 + 2q^{3/40} + q^{3/20} + 2q^{1/5} + 2q^{11/40} + q^{2/5} + 2q^{7/8}\right. \\
&\qquad \left. + 2q^{19/20} + O(q^{43/40})\right]
\end{aligned}
$$

Similarly, in the case of the model built on $D_4 \otimes D_4$, the modular invariant partition functions are given by

$$\text{branch one} : (D_4, A_6) \times (D_4, A_6) \qquad \text{branch two} : (A_4, D_4) \times (A_4, D_4)$$

and in the case of the model built on $A_5 \otimes D_4$ by

$$\text{branch one} : (A_5, A_6) \times (D_4, A_6) \qquad \text{branch two} : (A_4, A_5) \times (A_4, D_4).$$

All of our numerical results are consistent with the conjectured modular invariant partition functions summarized in section 1.

5. Conclusion

We have presented numerical evidence that the critical dilute A–D–E lattice models in the $u > 0$ branches provide a realization of both the (A, G) and the (G, A) series of modular invariant partition functions in the classification of Cappelli *et al* [1]. In the $u < 0$ branches

we have seen that the modular invariant partition functions are products of the (A_2, A_3) partition function with members of the (A, G) and (G, A) series. Furthermore, we have seen that the modular invariant partition functions of the two-colour A–D–E lattice models at criticality are squares of members of the (A, G) and (G, A) series.

Since these are all exactly solvable models, it would be interesting to see some exact calculations of scaling dimensions to compare with the predicted values. Indeed, such calculations have been performed in the case of the dilute A models in [13, 16].

Here we have only considered unitary minimal conformal field theories. It would also be interesting to see whether, by varying the crossing parameter, the dilute A–D–E lattice models might provide realizations of non-unitary minimal conformal field theories.

Acknowledgments

We thank Jean-Bernard Zuber for pointing out Roche's conjecture (3.19), Omar Foda for numerous discussions, and Ole Warnaar for helpful suggestions. This research is supported by the Australian Research Council.

References

[1] Cappelli A, Itzykson C and Zuber J-B 1987 *Nucl. Phys.* B **280** 445; 1987 *Commun. Math. Phys.* **113** 1
[2] Warnaar S O, Nienhuis B and Seaton K A 1992 *Phys. Rev. Lett.* **69** 710
[3] Roche Ph 1992 *Phys. Lett.* **4B** 929.
[4] Warnaar S O, Pearce P A, Seaton K A and Nienhuis B 1994 *J. Stat. Phys.* **74** 469
[5] Pasquier V 1987 *Nucl. Phys.* B **28** 162; 1987 *J. Phys. A: Math. Gen.* **20** L1229, 5707
[6] Warnaar S O and Nienhuis B 1993 *J. Phys. A: Math. Gen.* **26** 2301
[7] Belavin A A, Polyakov A M and Zamolodchikov A B 1984 *Nucl. Phys.* B **241** 333
[8] Friedan D, Qiu Z and Shenker S 1984 *Phys. Rev. Lett.* **52** 1575; 1984 *Vertex Operators in Mathematics and Physics* ed J Lepowsky, S Mandelstam and I M Singer (New York: Springer)
[9] Cardy J L, 1986 *Nucl. Phys.* B **270** 186; 1986 *Nucl. Phys.* B **275** 200
[10] Andrews G E, Baxter R J and Forrester P J 1984 *J. Stat. Phys.* **35** 193
[11] Huse D A 1984 *Phys. Rev.* B **30** 3908
[12] Warnaar S O, Batchelor M T and Nienhuis B 1992 *J. Phys. A: Math. Gen.* **25** 3077
[13] Zhou Y-K and Pearce P A 1995 Conformal weights of dilute A-lattice models, in preparation
[14] Kim D and Pearce P A 1987 *J. Phys. A: Math. Gen.* **20** L451
[15] Blöte H W J, Cardy J L and Nightingale M P 1986 *Phys. Rev. Lett.* **56** 742
Affleck I 1986 *Phys. Rev. Lett.* **56** 746
[16] Pearce P A and Zhou Y-K 1995 Unitary minimal conformal weights of dilute A-lattice models *Proc. Int. Congr. of Mathematical Physics (Paris)* to appear